Available online at www.sciencedirect.com
SCIENCE DIRECT
Earth and Planetary Science Letters 241 (2006) 119–137
EPSL
www.elsevier.com/locate/epsl

Magnetite dissolution, diachronous greigite formation, and secondary magnetizations from pyrite oxidation: Unravelling complex magnetizations in Neogene marine sediments from New Zealand

Christopher J. Rowan *, Andrew P. Roberts

National Oceanography Centre, Southampton, European Way, Southampton SO14 3ZH, United Kingdom

Received 19 April 2005; received in revised form 5 July 2005; accepted 14 October 2005
Available online 28 November 2005
Editor: V. Courtillot

Abstract

Detailed rock magnetic and electron microscope analyses indicate that the magnetic signature of Neogene marine sediments from the east coast of New Zealand is dominated by the authigenic iron sulphide greigite. The greigite is present as a mixed population of stable single domain and superparamagnetic grains, which is consistent with authigenic growth from solution. This growth can result from pyritization reactions soon after deposition, which also leads to dissolution of most detrital magnetite; however, where constrained by field tests, our data suggest that remanence acquisition can occur >1 Myr after deposition, and can vary in timing at the outcrop scale. Strong viscous overprints result from oxidation of the iron sulphides, probably during percolation of oxic ground water. This process can sometimes destroy any ancient remanent magnetization. This complex magnetic behaviour, particularly the presence of late-forming magnetizations carried by greigite, means that the remanence in New Zealand Cenozoic sediments, and in similar sediments elsewhere, cannot be assumed to be primary without confirmation by field tests. The reversals test should be employed with caution in such sediments, as patchy remagnetizations can lead to false polarity stratigraphies.

Keywords: magnetite; dissolution; greigite; pyrite; hematite; remagnetization; New Zealand

1. Introduction

Thick sequences of tectonically uplifted, fine-grained Cenozoic marine sediments from the Hikurangi Margin, on the east coast of New Zealand (Fig. 1a), provide standard mid-latitude sections for foraminiferal biostratigraphy. Since the 1970s, paleomagnetic data have been used to tie these sequences to the geomagnetic polarity timescale [1–3], enabling precise correlation of Neogene paleoclimatic variations in the southwest Pacific with changes in the Mediterranean and elsewhere [3]. Paleomagnetic data have also revealed substantial tectonic rotations of the Hikurangi Margin during the Neogene [4–11] and are crucial in linking past deformation to contemporary vertical axis rotations revealed by geodetic measurements [12,13]. However, despite over 30 yr of paleomagnetic research, long-standing questions concerning the origin of the magnetic signal in these sediments remain unanswered. Magnetic extractions often fail to clearly identify any

* Corresponding author.
E-mail address: cjr01@noc.soton.ac.uk (C.J. Rowan).

0012-821X/$ - see front matter © 2005 Elsevier B.V. All rights reserved.
doi:10.1016/j.epsl.2005.10.017

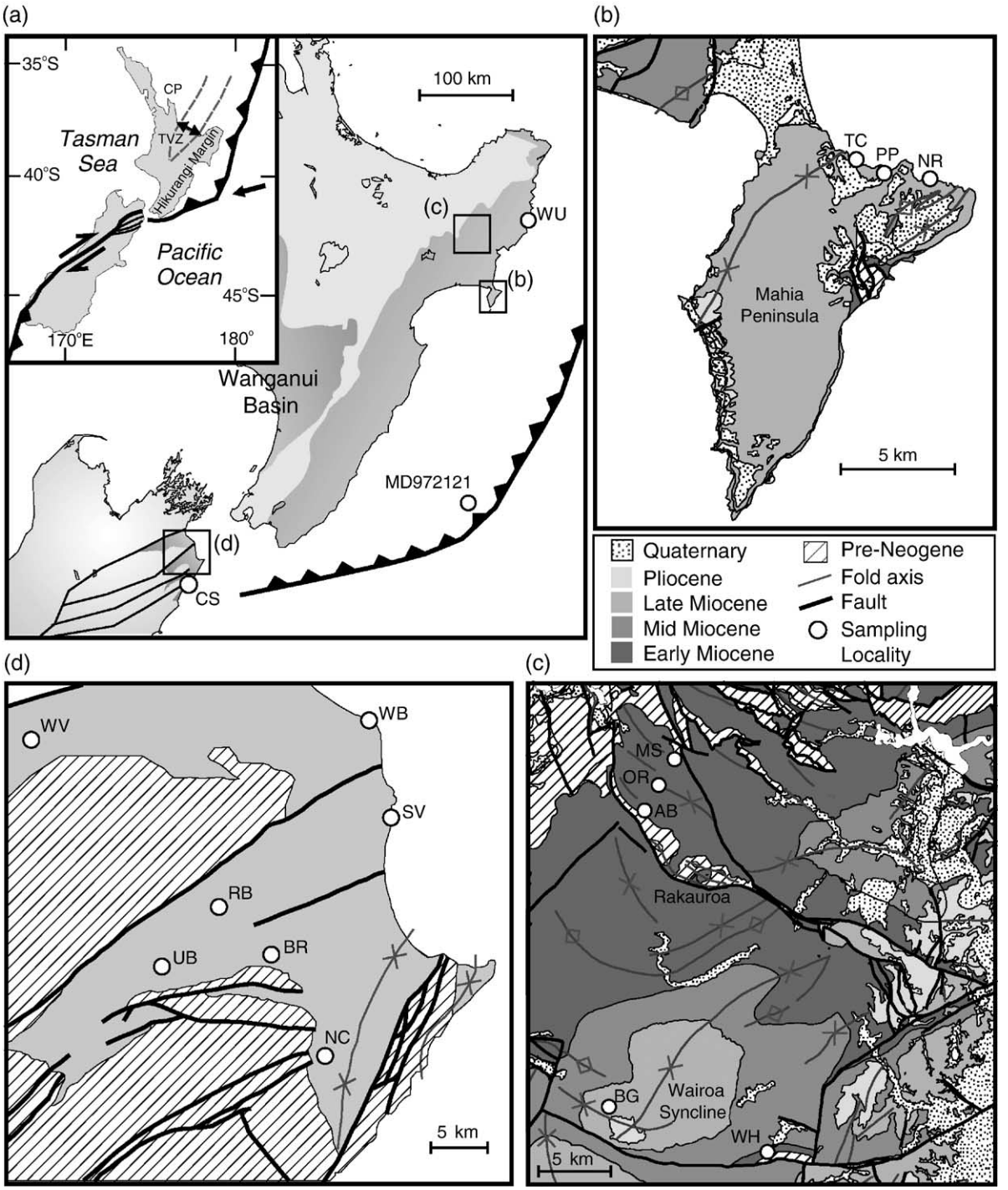

Fig. 1. Distribution of sampling localities. (a) Tectonic setting of the New Zealand region. Inset: boundary between the Australian and Pacific plates. TVZ = Taupo Volcanic Zone, CP = Coromandel Peninsula. Main figure: shaded regions delineate Neogene marginal basins. WU = Waihau Beach, CS = Camp Stream. The location of piston core MD972121 [21] is also shown. (b) Gently folded late Miocene sequences on the Mahia Peninsula. TC = Te Waipera Cemetery, PP = Putiki Point, NR = Nukutaurua Road. (c) Early Miocene–Pliocene sequences in the vicinity of the Wairoa Syncline. MS = Matawai Station, OR = Oliver Road, AB = Anzac Bridge, BG = Burgess Road, WH = Waterfall Hill. (d) Late Miocene–Pliocene (not subdivided on map) Awatere Group sediments, bounded by faults of the Marlborough fault system. WV = Waihopai Valley, WB = White Bluffs, SV = Sea View, RB = Richmond Brook, UB = Upton Brook, BR = Blind River, NC = Needles Creek. Figures in (b and c) are adapted from the QMAP data set [39], and (d) is modified from [10].

remanence-bearing phases that could be the carrier of their weak (typically 10^{-5}–10^{-3} A m^{-1}) natural remanent magnetization (NRM) [14]. Alternating field (AF) demagnetization is often unsuccessful in isolating a stable characteristic remanent magnetization (ChRM), and the results of thermal demagnetization indicate low unblocking temperatures (250–350 °C) that are consistent with a wide range of possible magnetic minerals. Establishing the origin of a strong, widespread, present-day field overprint has also proven problematic.

Neogene sedimentary sequences from the Hikurangi Margin were principally deposited in marginal basin settings since the initiation of subduction at 20–23 Ma [15,16], and ongoing shortening along the subduction system has led to their uplift above sea level. The sediments were chiefly sourced from uplifted Triassic–Cretaceous basement rocks of the Torlesse Supergroup, which have been through repeated cycles of uplift, erosion and redeposition [17]; exposure to anoxic diagenetic conditions during such cycles makes these rocks a poor source of detrital magnetic iron oxides such as magnetite [18,19]. Since the mid-Miocene, increasing amounts of detrital iron oxides have been supplied to marginal basins by volcanic activity on the Coromandel Peninsula, and, since 2 Ma, from the Taupo Volcanic Zone [20]. Evidence of recent volcanic activity is apparent in the magnetic signature of Holocene sediments from the continental slope east of the North Island (Figs. 1a, 2), where peaks in NRM intensity at the top of core MD972121 (Fig. 2a) correlate to ash layers rich in detrital magnetic minerals [21]. However, below 4.7 m depth no such peaks occur, and from 4.2 to 4.7 m, there is also a substantial, permanent drop in the background NRM intensity (Fig. 2a), accompanied by a significant decrease in its median destructive field (MDF) below 3 m (Fig. 2b). Following the onset of anoxic conditions, iron-bearing minerals such as magnetite will react with H_2S, produced by bacterial reduction of sulphate during the decomposition of organic matter, forming pyrite (FeS_2) [22] (Fig. 2c). Within about 12,000 yr of deposition most detrital magnetic minerals in core MD972121, even in the magnetite-rich ash layers, have been dissolved, particularly magnetically stable single-domain (SD) grains. All that remains is a sparse population of multi-domain grains (with low MDFs) that are unlikely to record a stable remanent magnetization. As reported by Karlin and Levi [23,24] and Karlin [25], this type of signature is common in organic-rich, terrigenous sediments from continental margins.

The effects of pyritization are not only evident in modern sediments. Pyrite is abundant in the uplifted Neogene sequences of New Zealand, and magnetic extractions have yielded abundant paramagnetic ilmenite, which is more resistant to dissolution than ferrimagnetic iron oxides [26], but only minor amounts of titanomagnetite [14,19,27] (occasional exceptions exist, e.g., Little and Roberts [11] reported magnetite in sedi-

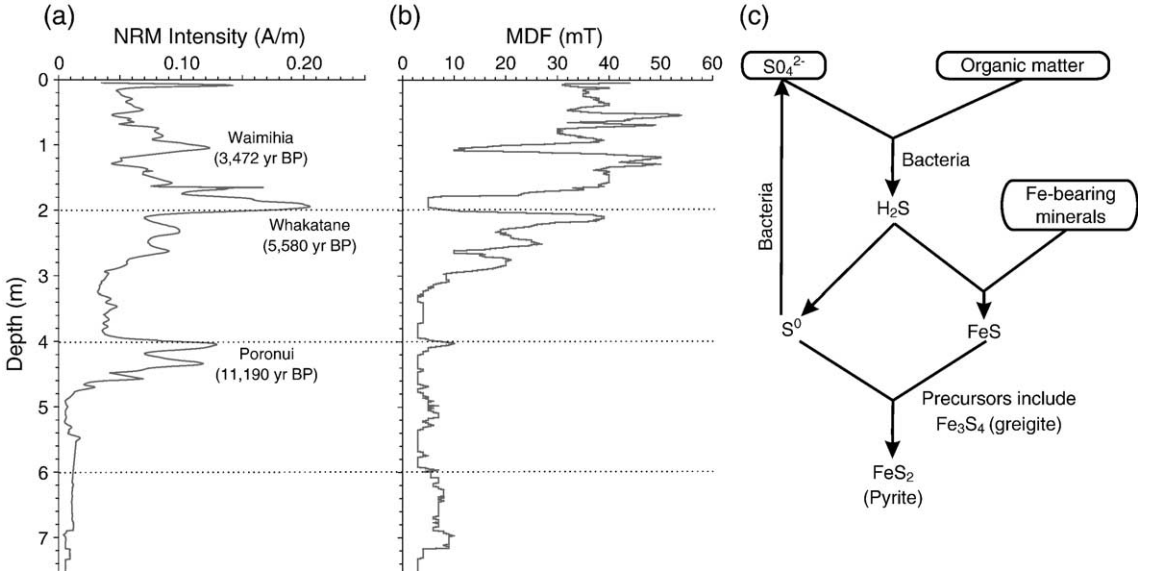

Fig. 2. Down-core profiles of (a) NRM intensity and (b) median destructive field (MDF) for piston core MD972121 [21]. In the upper 4.7 m of the core, NRM peaks and corresponding MDF minima correlate with dated ash layers rich in coarse magnetic minerals. Below 4.7 m, NRM and MDF both decrease significantly, indicating dissolution of detrital magnetic minerals; susceptibility profiles for the entire 35 m core (not shown) indicate that this reduction is permanent. (c) Pyritization reactions, after [22].

ments that were probably partially sourced from Cretaceous volcanics). Typical depositional environments in marginal basins of the Hikurangi Margin have apparently been consistently inimical to the preservation of detrital magnetite since the Early Miocene, and it is therefore unlikely to be a significant contributor to the remanence of most of these sediments.

Pyritization proceeds via a series of precursors that include the ferrimagnetic iron sulphide greigite (Fe_3S_4) [22,28]. Although it is generally regarded as metastable, instances of greigite carrying a stable ChRM are increasingly being recognized in the geological record [29]. It has been shown that where reactive iron is abundant and organic carbon is relatively restricted, any dissolved sulphide reacts rapidly with available dissolved iron, which can lead to incomplete pyritization and the preservation of greigite [30]. Such conditions are particularly likely to arise where the sedimentation rate, and therefore the dilution of organic matter by terrigenous material, is high.

In New Zealand, greigite has previously been reported in a small part of a late Miocene section in Marlborough [19] (UB, Fig. 1d) and, more recently, in early late Miocene rocks from the northern Hikurangi Margin [31] (WU, Fig. 1a). Greigite has also been inferred to be present in Pleistocene sediments from the Wanganui Basin, western North Island [32]. Although definitive identifications of greigite have only been made in these few instances, the demagnetization behaviour of samples from the localities in question is consistent with that of paleomagnetic samples from similar sediments throughout New Zealand [14], which raises the possibility that authigenic greigite is a common remanence carrier in these rocks. The steady-state diagenetic model of Berner [22] confines pyritization reactions to the top of the sediment column, in which case any remanence carried by greigite will record the geomagnetic field close to the time of deposition. However, increasing reports of later forming greigite [29,33–35], including one instance within New Zealand itself [31], make it clear that external forcing events can potentially change pore water chemistry and trigger greigite formation at any time after deposition, not just during initial reductive diagenesis. In New Zealand, paleomagnetic data from Cenozoic sediments are rarely constrained by rigorous field tests; if greigite is a common remanence carrier, the possibility of late-forming magnetizations becomes an issue of real concern.

In this study, we discuss paleomagnetic results from samples collected along the length of the Hikurangi Margin. The complex behaviour observed, particularly the abundance of late-forming magnetizations, is consistent with the presence of an authigenic mineral; we present rock magnetic and scanning electron microscope (SEM) observations that confirm in all cases that this mineral is greigite. Later oxidation of iron sulphides can also be implicated in the formation of strong viscous overprints. We then address the implications of these results, not only for paleomagnetic studies in New Zealand, but also in similar tectonically active marginal basins around the Pacific, the Mediterranean, and other areas that are host to rapidly deposited terrigenous sediments and reducing diagenetic environments.

2. Sampling and methods

The majority of the results presented here come from a comprehensive paleomagnetic sampling program undertaken in 2002–2003 in order to study the tectonic evolution of the Hikurangi Margin. Paleomagnetic analysis of samples from over 40 localities was performed using a 2G-Enterprises cryogenic magnetometer, situated in a magnetically shielded room at the National Oceanography Centre, Southampton (NOCS). Samples were stepwise demagnetized using both thermal (40° steps from 80 °C to 400 °C) and AF (5-mT steps to 60 mT) techniques. These measurements reveal a wide range of paleomagnetic behaviours, including strong present-day field overprints [36] and differently timed magnetizations separated by several million years [31]. We have focused on a subset of these localities, chosen to reflect this variety, for further investigations of magnetic mineralogy (Fig. 1, Table 1). Samples from earlier studies in the Marlborough region (Fig. 1d) [3,10] are also included. Three types of analysis were performed: (a) measurement of the bulk magnetic hysteresis properties of ~1-cm^3 sub-samples, using a Princeton Measurements Corporation Micromag 3900 vibrating sample magnetometer (VSM) at NOCS. Values of saturation magnetization M_s, saturation remanent magnetization M_r, and coercive force B_c were obtained from hysteresis loops (0.5 T saturating field); the coercivity of remanence B_{cr} was determined from back-field remanence curves. (b) Measurement of first-order reversal curves (FORCs), which are a class of partial hysteresis loop measured by cycling between a positive saturation field and a reversal field B_a [37,38], using the same VSM. A series of FORCs with different B_a values provides a more complete sampling of the magnetic response of the sample than a single hysteresis loop; this information is commonly represented on a FORC diagram, which is a contour plot of the coercivity

Table 1
Magnetic properties of samples analyzed in this study

Locality	n	NRM intensity ($\times 10^{-4}$ A m^{-1})	NRM $>5\times10^{-4}$ A m^{-1} (%)	Hysteresis ratios		
				n	M_r/M_s	B_{cr}/B_c
Mahia Peninsula (Fig. 1b)						
TC	54	2.7–34	89	15	0.12–0.52	1.35–3.90
PP	42	0.5–12	24	4	0.20–0.24	3.23–3.72
NR	83	0.2–64	19	21	0.03–0.20	3.13–17.47
Rakauroa (Fig. 1c)						
MS	60	0.1–2.2	0	2	0.12–0.13	2.93–3.21
OR	81	0.5–7.6	9	2	0.17–0.18	2.70–2.85
AB	42	0.5–1.8	0	2	0.12–0.14	3.64–3.84
Coast North of Gisborne (Fig. 1a)						
WU	60	0.2–15	7	8	0.13–0.19	3.38–3.87
Wairoa Syncline (Fig. 1c)						
WH	16	2.2–5.3	6	2	0.13–0.14	3.67–3.99
BG	11	3.4–7.8	44	2	0.11–0.13	4.96–5.61
Marlborough (Fig. 1a and d)						
SV	12	16–41	100	3	0.28–0.41	1.64–2.59
UB	19	1.3–93	55	6	0.14–0.59	1.27–3.46
WB	14	0.3–22	7	3	0.23–0.49	1.38–2.56
BR	9	1.5–4.1	0	2	0.14–0.16	3.51–3.75
CS	12	1.0–44	58	2	0.36–0.45	1.46–1.75
RB	12	1.1–27	75	3	0.22–0.44	1.35–2.34
WV	12	1.1–16	42	2	0.14–0.15	3.19–3.20
NC	10	1.9–26	70	3	0.14–0.33	1.78–3.60

Locality names are abbreviated as in Fig. 1. n=number of samples analyzed; NRM=natural remanent magnetization; M_r=saturation remanent magnetization; M_s=saturation magnetization; B_{cr}=coercivity of remanence; B_c=coercive force.

distribution of magnetic particles and their interaction field strengths [37,38]. We measured 140 FORCs for each sample, with a field spacing of 1.85 mT and an averaging time of 250 ms, in a 0.5-T saturating field. FORC distributions were calculated using a smoothing factor (SF) of 5. (c) SEM observations of resin-impregnated polished sections, combined with elemental analysis of mineral phases using an X-ray energy dispersive spectrometer (EDS). Principal observations were made at NOCS using a LEO 1450VP SEM, operated at 10–20 keV with an acceleration voltage of 17–20 pA, and a Princeton Gamma Tech (IMIX-PTS) EDS system. Some supplementary analyses were made with a JEOL JSM-6360LV SEM, operated at 15 keV with an 18-pA acceleration voltage, and an Oxford Instruments Ltd INCA-300 EDS, at the Institute of Earth Sciences, Academia Sinica, Taipei, Taiwan. Observations focused on iron sulphides, which are easily identified by their high electron backscatter. Careful analysis of EDS measurements, calibrated with a pyrite standard, allows different phases such as greigite and pyrite to be distinguished by their distinctive iron to sulphur ratios (Fe/S=0.75 and =0.5, respectively) [29,31,33,35].

3. Paleomagnetic data

The diverse paleomagnetic behaviour of the studied sediments reflects the wide range of processes that have contributed to their complex magnetization. Results from the localities described below are representative examples of these various processes.

3.1. Differentially timed synfolding magnetizations, Mahia Peninsula

Three localities were sampled within a thick sequence of fine-grained mudstones, interbedded with tuffs and reworked tuffaceous beds, on the north coast of Mahia Peninsula (Fig. 1b). The rocks are all of late Miocene (6.5–11.0 Ma) age [39] and are distributed across a syncline formed during early Pliocene folding [40].

Near Te Waipera Cemetery (locality TC), we sampled a 24.0-m sequence consisting of massive, dark grey, fine-grained mudstones, overlain by interbedded mudstones and tuffaceous beds, with one primary tuff (Fig. 3a). The bedding attitude is 203/10 NW (Fig. 1b).

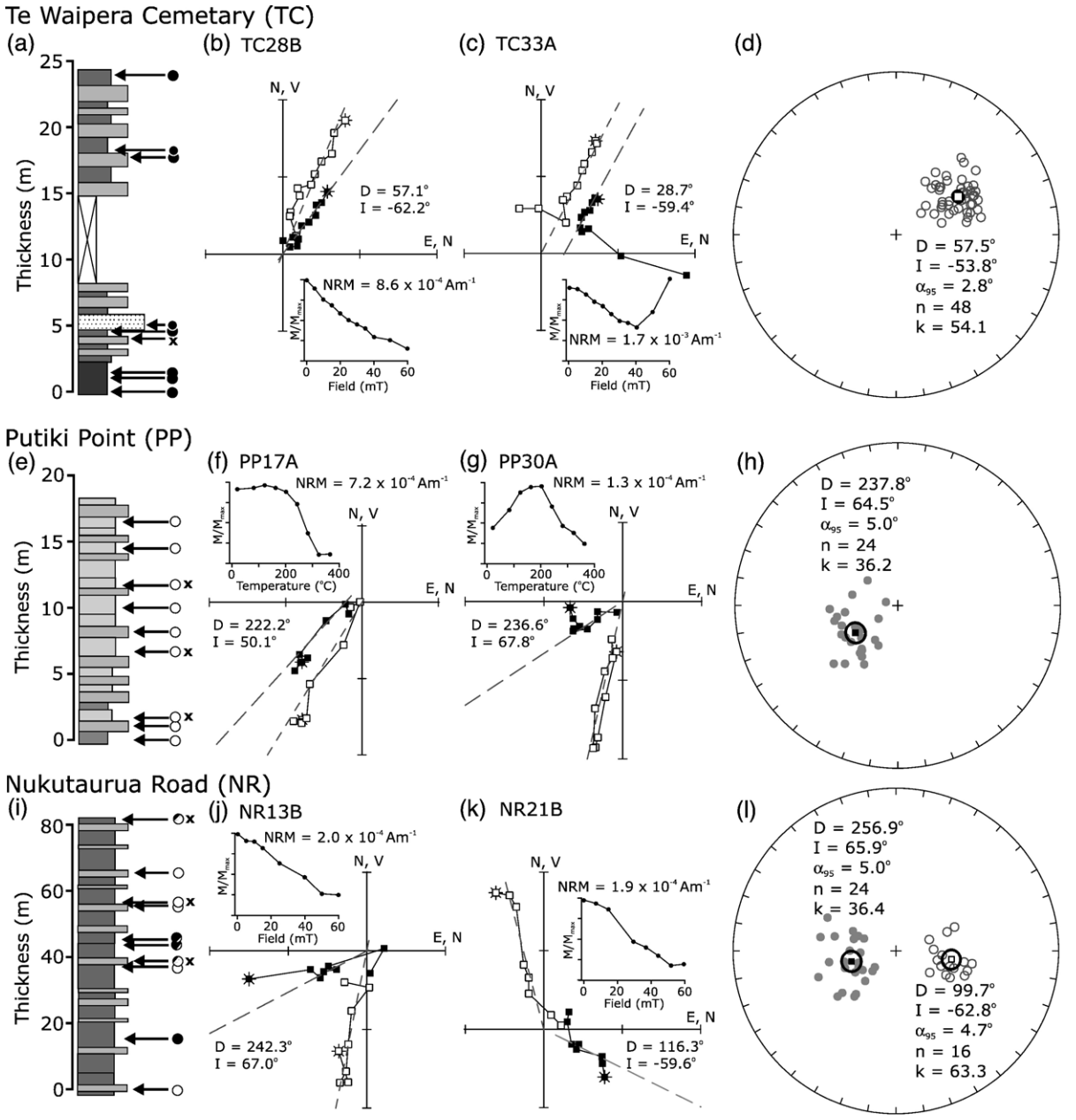

Fig. 3. Paleomagnetic data from Mahia Peninsula. (a) Sequence sampled at locality TC. Arrows mark sampling horizons in mudstones (black and dark grey) and tuffaceous beds (light grey, and stipple for primary tuff). Horizons with normal polarity (solid circle) or unstable magnetization (cross) are indicated. (b) Vector component plot of AF demagnetization data for sample TC28B. Solid symbols denote declinations, open symbols denote inclinations, dashed lines show best-fit directions from principal component analysis. (c) AF demagnetization data for sample TC33A, with GRM acquisition above 40 mT. (d) Equal area stereographic projection of normal polarity ChRM directions (open circles) from TC, and the calculated mean direction with α_{95} error ellipse (bold). (e) Sequence sampled at locality PP. All sampling horizons had reversed polarity magnetizations (open circles), with unstable ChRMs at three levels (crosses). (f) Thermal demagnetization data for sample PP17A. (g) Thermal demagnetization data for sample PP30A, with a strong normal polarity overprint and reversed ChRM. (h) Stereoplot of reversed polarity ChRMs (closed circles) from PP, with calculated mean direction. (i) Sequence sampled at locality NR, showing distribution of normal and reversed polarity and unstably magnetized horizons. Partially open/closed circles mark horizons with samples of both polarities. (j) AF demagnetization data for reversed polarity sample NR13B. (k) AF demagnetization data for normal polarity sample NR21B. (l) Stereoplot of normal and reversed polarity ChRMs from NR, with calculated mean directions.

NRMs are strong, with intensities $>5\times10^{-4}$ A m^{-1} in 89% of samples (Table 1), and a minimally overprinted, normal polarity ChRM was almost universally recovered (Fig. 3b and c). Thermal and AF demagnetizations were both effective, although AF-treated samples from the lower part of the section often developed a strong gyroremanent magnetization (GRM) above 40 mT (Fig. 3c). After correction for bedding tilt, 48 samples yielded a mean paleomagnetic direction of declination (D)=57.5°, inclination (I)=−53.8°, α_{95}=2.8° (Fig. 3d).

At Putiki Point (locality PP), the 16.5-m sequence sampled consists of shallowly dipping (bedding attitude 239/11 NW) white, ash-rich mudstones, with minor reworked tuff beds (Fig. 3e). In comparison to TC, samples had weaker NRMs, with 76% of samples having intensities $<5\times10^{-4}$ A m^{-1} (Table 1), and AF demagnetization was generally ineffective. A reversed polarity ChRM was isolated from 24 samples, producing a mean direction in tilt-corrected coordinates of D=237.8°, I=64.5°, α_{95}=5.0° (Fig. 3h). The ChRM was overprinted to various degrees by a normal polarity component (Fig. 3f and g), which was so strong at three sampling levels that a stable endpoint could not be isolated (marked by crosses in Fig. 3e).

At the end of Nukutaurua Road (locality NR), we sampled an 81.5-m sequence of more steeply dipping (bedding attitude 240/48 NW) pale grey mudstones, regularly interbedded with white reworked tuffs (Fig. 3i). NRMs were generally weak (81% of samples $<5\times10^{-4}$ A m^{-1}) and noisy demagnetization paths were common; at three horizons, the remanence was so unstable that reliable directions could not be isolated (Fig. 3i). Both normal and reversed polarity ChRMs were identified in this section (Fig. 3j and k). After tilt correction, a mean direction of D=99.7°, I=−62.8°, α_{95}=4.7° was determined from 16 normal polarity samples; the mean reversed polarity direction was D=256.9°, I=65.9°, α_{95}=5.0° from 24 samples (Fig. 3l).

In tilt-corrected coordinates, the normal and reversed polarity mean directions from NR fail the reversals test (critical angle at 95% confidence level=7.0°; observed angle between means=10.3°) [41]. The reversed polarity direction is close to that isolated at PP, although it fails the test for a common mean (critical angle=6.2°; observed angle=8.1°) (Fig. 4a), but the normal polarity direction has a significantly higher declination than the mean direction from TC. Reversing the tilt correction

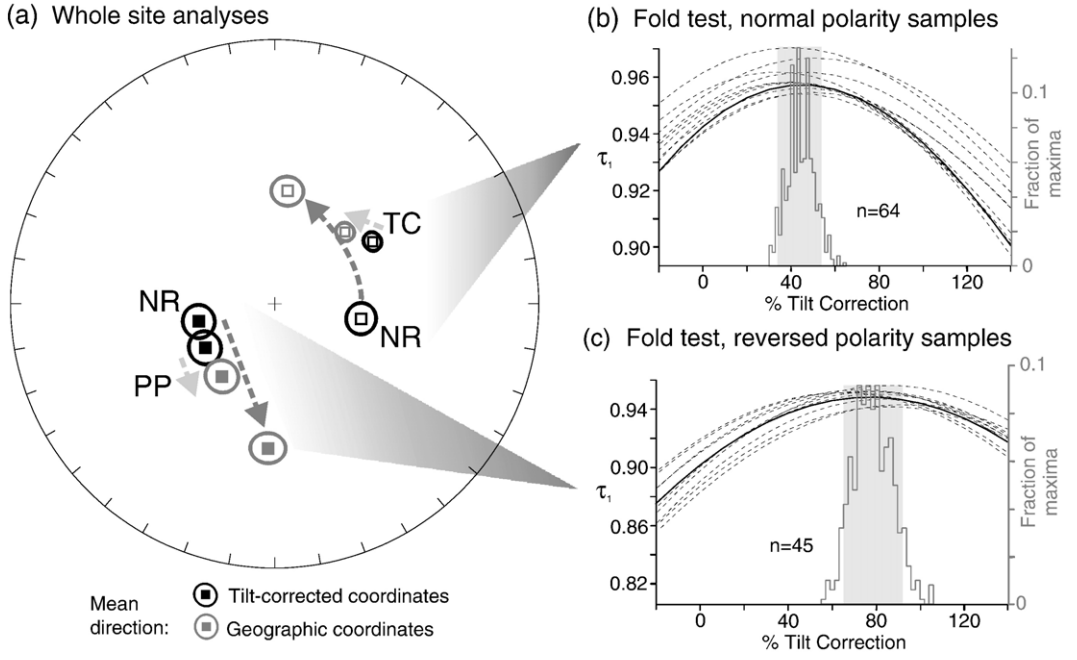

Fig. 4. (a) Calculated mean directions and α_{95} error ellipses in both geographic and tilt-corrected coordinates for the TC, PP, and NR localities, Mahia Peninsula. Dashed arrows demonstrate how the directions from the different localities are brought into better agreement by reversing the tilt correction. (b) Bootstrap fold test of [42], applied to normal polarity ChRMs from TC and NR. Variation of the principal eigenvector τ_1 with various degrees of unfolding is depicted with dashed lines for different para-data sets; the distribution of maxima for these data sets is shown by the histogram. The 95% confidence interval (grey shading) puts the maximum at 34–54% unfolding, indicating a synfolding magnetization. (c) Fold test applied to reversed polarity ChRMs from PP and NR. The 95% confidence interval for the maximum value of τ_1 is at 65–92% unfolding, indicating a synfolding magnetization acquired earlier than the normal polarity remanence.

restores the mean directions from the moderately tilted NR locality closer to those from the other two localities (Fig. 4a), but less tilting is required to reconcile the reversed polarity data. This suggests that the two polarities represent differently timed, synfolding magnetizations. The presence of sister samples with different polarities in several horizons in the middle of the NR section (Fig. 3i) suggests that the polarity sequence is not primary, which supports the hypothesis of differential timing. Applying the fold test of Tauxe and Watson [42] separately to the normal and reversed polarity directions (Fig. 4b and c) produces a clear difference at the 95% confidence level: the reversed polarity directions are in best agreement at 79% unfolding, while the normal polarity directions cluster at 44% unfolding. The normal polarity magnetization was therefore acquired demonstrably later, although both polarities are clearly associated with the same folding episode; there is no trace of a syndepositional remanence at any of the Mahia localities. Paleomagnetic mean directions after partial unfolding combine to give a declination of $49 \pm 5^\circ$ for the Mahia Peninsula localities; large-scale motion of the Australian plate accounts for 1°/Myr of clockwise rotation [43], leaving a declination anomaly of $44 \pm 5^\circ$ since folding at 4–6 Ma.

3.2. Early forming magnetization, Rakauroa region

As reported by Rowan et al. [36], resampling of three Early Miocene localities in the Rakauroa region (Fig. 1c) established that a previously reported large declination anomaly [5] was the result of incomplete removal of a large viscous overprint. At Oliver Road (OR) and Matawai Station (MS), more rigorous analysis yielded tectonically unrotated, reversed polarity declinations (Table 2), which are shown by field tests to predate early folding. At Anzac Bridge (AB), the remaining site, no stable ChRM could be isolated beneath the overprint. The OR and MS localities represent a clear instance of an early-forming remanence that preserves a retrievable ChRM despite strong overprinting. NRM intensities were $<5 \times 10^{-4}$ A m^{-1} for almost all samples at these localities.

3.3. Early and late magnetization, Waihau Beach

Two distinct magnetizations with opposite polarity, both with weak NRM intensities (7% of samples having intensities $>5 \times 10^{-4}$ A m^{-1}), and with a 60° difference in declinations, were reported from a section of massive, grey mudstone, with interbedded tuffaceous layers, at Waihau Beach (WU) (Fig. 1a; Table 2). The large discrepancy in declinations can only be accounted for if several million years of vertical-axis rotation has occurred between the acquisition of these two magnetizations [31]. The later forming, reversed polarity remanence has only patchily grown within the section, which results in an apparent reversal sequence. SEM observations confirm that both polarities are chemical remanent magnetizations (CRMs) carried by greigite [31].

Table 2
Summary of paleomagnetic results

Locality	D (°)	I (°)	α_{95} (°)	k	Reference
Mahia Peninsula (Fig. 1b)					
TC[a]	57.5	−53.8	2.8	54.1	This study
	99.7	−62.8	4.7	63.3	
NR[a]	256.9	65.9	5.0	36.4	This study
PP[a]	237.8	64.5	5.0	36.2	This study
Rakauroa (Fig. 1c)					
MS	198.9	43.3	8.1	12.6	[36]
OR	195.5	47.5	5.8	16.3	[36]
AB	Present day field				[36]
Coast North of Gisborne (Fig. 1a)					
WU	85.6	−49.5	4.5	55.5	[31]
	206.8	63.1	7.0	18.7	
Wairoa Syncline (Fig. 1c)					
WH	Present day field				This study
BG	Present day field				This study
Marlborough (Fig. 1a and d)					
SV	223.5	58.7	3.1	67.1	[10]
UB	201.3	59.0	1.8	48.2	[10]
WB	204.2	67.0	3.6	58.1	[10]
BR	212.6	59.5	2.0	37.5	[10]
CS	174.8	59.3	2.8	50.8	[10]
RB	211.6	61.8	3.9	56.5	[10]
WV	199.6	60.6	2.4	84.6	[10]
NC	215.4	59.8	3.5	61.1	[10]

Mean directions are given in tilt-corrected coordinates.
[a] Localities with synfolding magnetizations; these directions are therefore not indicative of tectonic rotations.

3.4. Strong present-day field overprint, Wairoa Syncline

Two localities were sampled across the Wairoa Syncline (Fig. 1c): a roadside outcrop of interbedded silty mudstones and sandstones, with a steep northwest dip, near Waterfall Hill (WH); and a section of massive, sandy mudstone with occasional sandstone beds exposed on the northern bank of the Hangaroa River near Burgess Road (BG). NRM intensities of samples from BG were higher than at WH (with 44% and 6% of samples $>5 \times 10^{-4}$ A m^{-1}, respectively). However,

demagnetization data indicate that both localities are dominated by a low-temperature, low-coercivity remanence component, which aligns with the present-day field direction ($D=20$, $I=-64°$) before tilt correction, indicating that it is a viscous overprint (Fig. 5). The low MDF and unblocking temperatures indicate that, in contrast to the nearby Rakauroa localities, no older paleomagnetic signal has been preserved, which is a common phenomenon in this region [8].

3.5. Marlborough

Extensive paleomagnetic sampling of fine-grained late Miocene to Pliocene sediments has been undertaken in the Marlborough region, at the southern end of the Hikurangi Margin (Fig. 1a and d), for tectonic [10,11] and stratigraphic [3,44] studies. Vertical axis rotations inferred from paleomagnetic data correlate well with deviations in the strike of a vertical structural fabric in the underlying Late Jurassic to Early Cretaceous Torlesse basement rocks [11], which suggests relatively early remanence acquisition dates.

Previously unanalyzed paleomagnetic samples from the collection of Roberts [10] provide a larger data set for interpreting the magnetic properties of Neogene sediments from New Zealand. Samples were stepwise AF demagnetized before preparation for VSM and SEM analyses. NRM intensities were generally higher than those observed in localities from the northern Hikurangi Margin, with an average of 51% of samples having intensities $>5\times10^{-4}$ A m^{-1} (Table 1). Although AF demagnetization was found to be generally ineffective in the original studies [44], directions comparable to previously published thermal demagnetization data (Table 2) were obtained from Upton Brook (UB), Sea View (SV), White Bluffs (WB), and Waihopai Valley (WV). At other localities, particularly Richmond Brook (RB), Needles Creek (NC) and Camp Stream (CS), lengthy storage (15 yr) in an unshielded environment appears to have led to the development of strong secondary overprints.

4. Rock magnetic and SEM observations

Greigite has already been clearly identified as a remanence carrier in samples from Upton Brook (UB) and Waihau Beach (WU), by X-ray diffraction (XRD) on magnetic separates [19] and SEM analyses of polished sections [31], respectively; this provides a useful starting point for our rock magnetic measurements. The FORC distribution for sample UB192A (Fig. 6a), which is from close to the stratigraphic interval where greigite was reported by Roberts and Turner [19], indicates a large population of strongly interacting SD grains with a peak coercivity of ~60 mT, which is typical of greigite [38]. In contrast, the distribution for sample WU21A lies closer to the origin of the FORC diagram, with a slight peak at ~20 mT (Fig. 6b). Such low coercivities have not previously been considered indicative of sedimentary greigite, which is generally associated with high coercivities of the type indicated in Fig. 6a [45]. A large peak at the origin of the FORC distribution in both samples, most easily seen in profiles along the B_c axis (Fig. 6c and d), indicates a

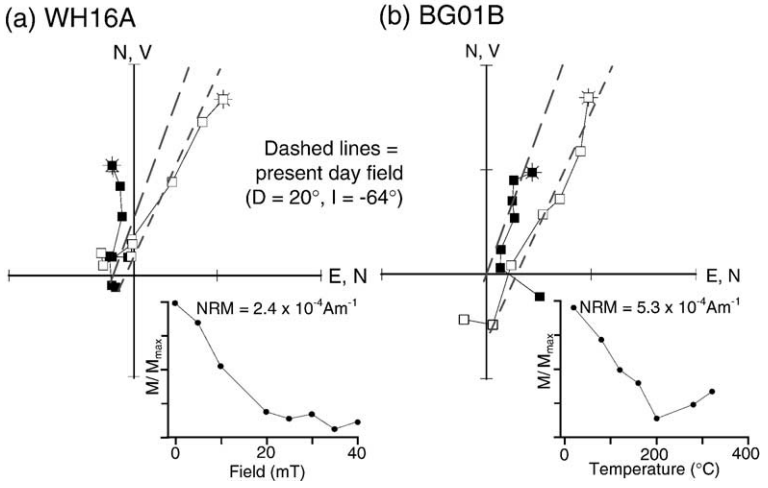

Fig. 5. Vector component plot of (a) AF demagnetization data for sample WH16A and (b) thermal demagnetization data for sample BG01B (symbols as in Fig. 3). Data are plotted before correction for bedding tilt and show only a low-coercivity, low-temperature component aligned with the present-day field (dashed lines) which is interpreted as a viscous overprint.

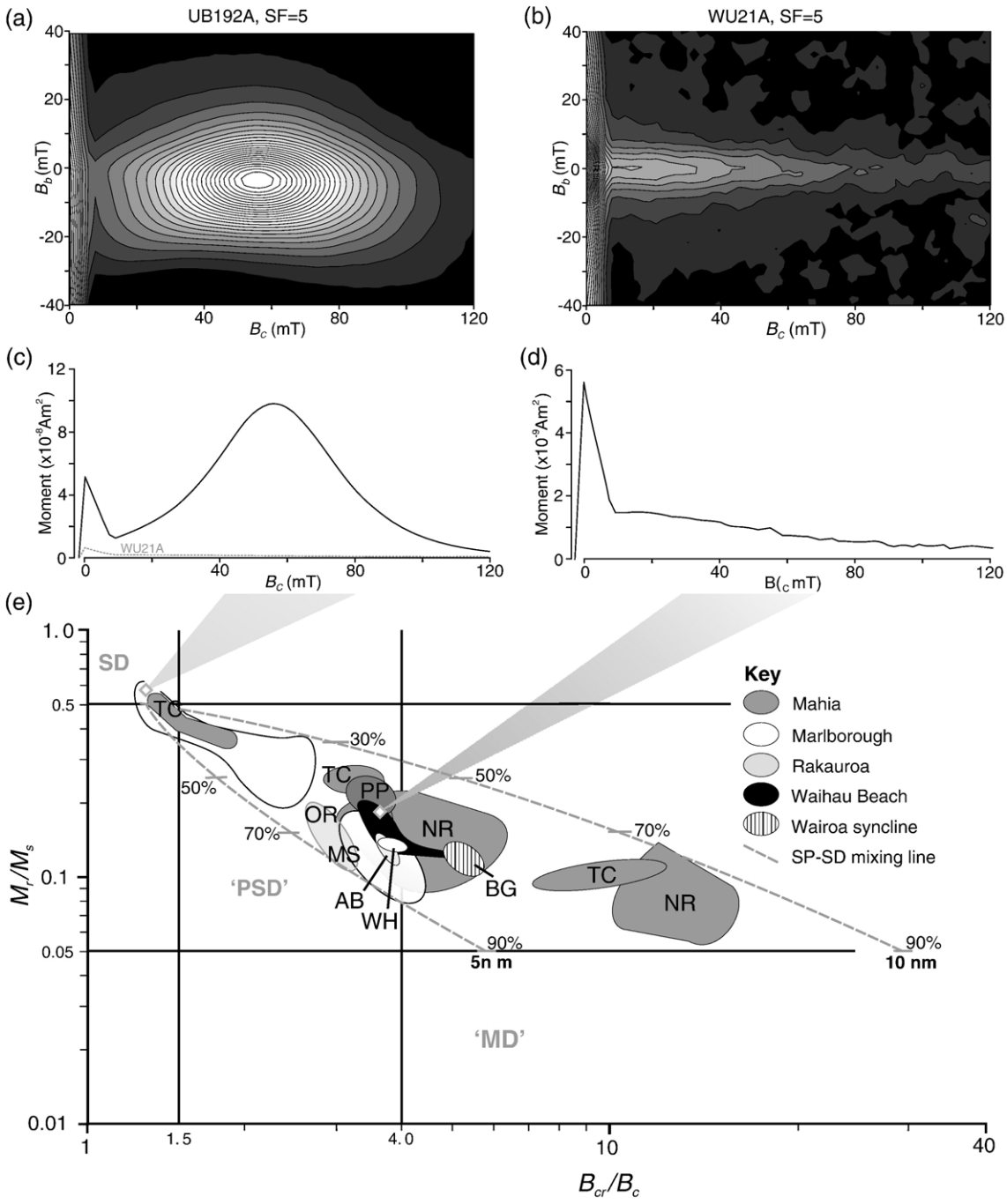

Fig. 6. (a and b) FORC distributions for samples UB192A and WU21A, which are both known to contain greigite, interpreted as (a) a population of SD greigite with strong magnetostatic interactions, and (b) a smaller population of SD greigite, with minimal interactions and a coercivity distribution shifted toward the origin by thermal relaxation. (c and d) Profiles through the FORC distribution at $\boldsymbol{B}_u = 0$ for both samples, illustrating the large reversible ridges at $\boldsymbol{B}_c = 0$. (e) Hysteresis parameters for all samples in this study, plotted according to Day et al. [50]. Compared to the SD-like values of sample UB192A, the large SP population of sample WU21A has reduced M_r/M_s and increased $\boldsymbol{B}_{cr}/\boldsymbol{B}_c$; many other samples from the Hikurangi Margin also plot in the same region. Theoretical curves for mixtures of SD and SP (titano)magnetite [49] have been plotted for 5-nm and 10-nm SP grains (% refers to % SP grains), although the assumption of a constant SP grain size is probably not valid in this case.

significant reversible component of magnetization due to paramagnetic and superparamagnetic (SP) particles [46]. Pike et al. [47] demonstrated that thermal relaxation in a population of SD grains will progressively shift a FORC distribution to lower B_c; in the extreme case of a sample dominated by SP particles, the FORC distribution will be centred on the origin of the FORC diagram [47]. It therefore appears that in addition to

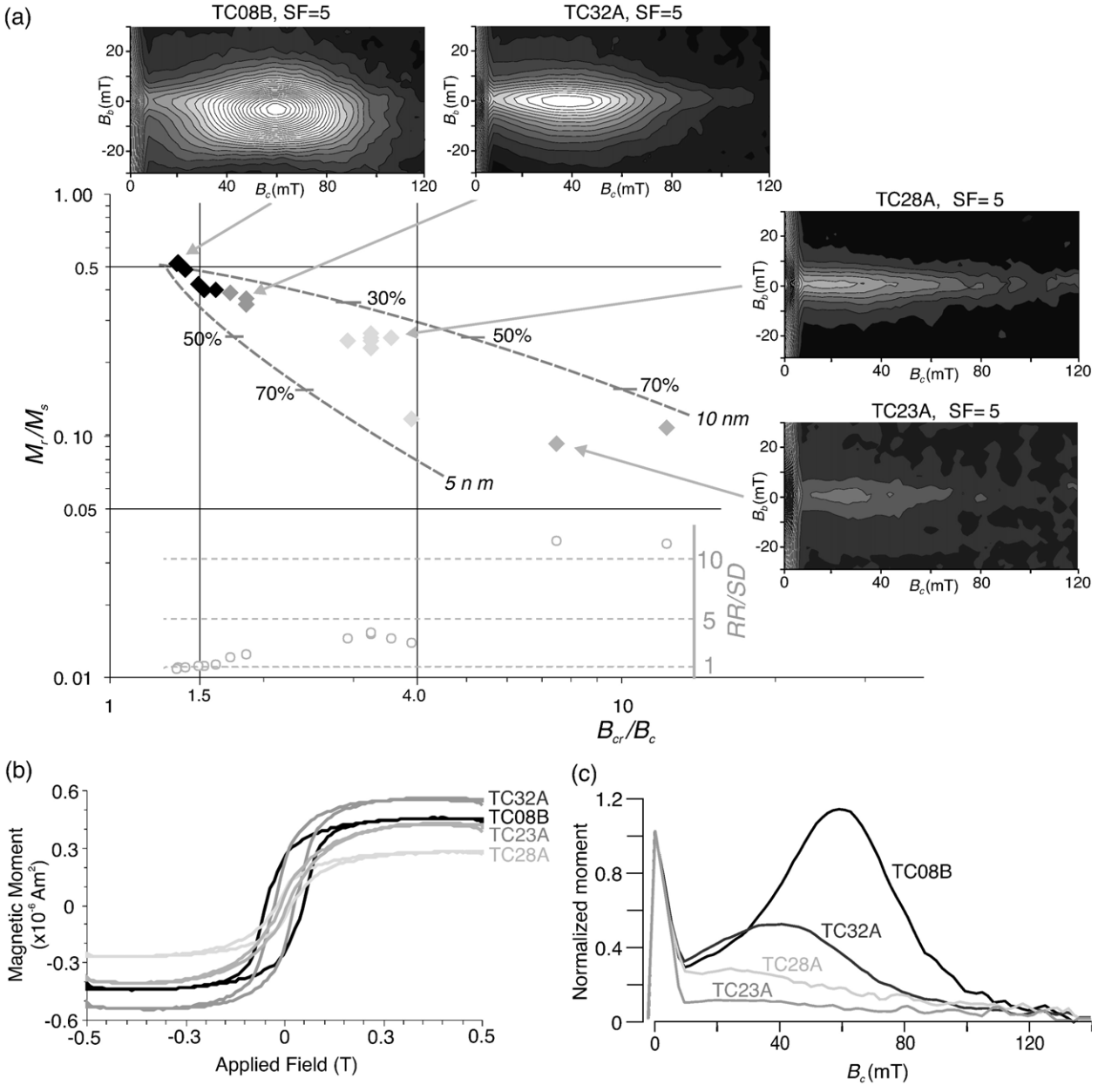

Fig. 7. (a) Day plot illustrating the relationship between varying hysteresis ratios and the FORC distributions of selected samples from locality TC. SD-SP mixing curves [49] are again plotted for reference. Decreasing M_r/M_s and increasing $\boldsymbol{B}_{cr}/\boldsymbol{B}_c$, consistent with an increase in SP content, accompany the lower coercivity distribution and increased thermal relaxation of the stable SD population on the FORC distribution. The relative magnitude of the reversible ridge at $\boldsymbol{B}_c=0$ also increases, as shown by the inset plot of *RR/SD*, the ratio of the heights of the reversible ridge and the SD peak. (b) Hysteresis loops for selected samples from (a), with the paramagnetic slope corrected. Samples with higher $\boldsymbol{B}_{cr}/\boldsymbol{B}_c$ (TC23A, 28A) are more wasp-waisted than samples with more SD-like values (TC08B, 32A), which is diagnostic of a larger SP contribution [48]. (c) Profiles along the $\boldsymbol{B}_c$ axis of FORC distributions from (a), normalized to the peak of the reversible ridge at $\boldsymbol{B}_c=0$. As the SD peak gets proportionally smaller, it also shifts toward the origin, due to thermal relaxation of the proportionally larger SP population.

stable SD greigite, sample WU21A contains a substantial SP population, which causes the FORC distribution to shift to lower coercivities and also contributes to a large reversible ridge (Fig. 6d).

Large SP populations will also alter bulk hysteresis parameters, decreasing M_r/M_s and markedly increasing B_{cr}/B_c [48,49], which is consistent with the position of sample WU21A on a Day [50] plot (Fig. 6e). A similar range of magnetic properties is exhibited by all samples in this study, which also have FORC distributions with a measurable reversible ridge at the origin consistent with the presence of a sizeable SP (or paramagnetic) contribution. On a Day plot, the samples follow a trend that resembles theoretical SD-SP mixing curves for (titano)magnetite [49] (Fig. 6e). Although strict numerical comparison with the results of Dunlop [49] cannot be made, the magnetic behaviour of SD-SP greigite mixtures broadly resembles that expected for (titano)magnetite mixtures. Changes in magnetic properties amongst these samples therefore appear to be linked to a change in the relative proportions of thermally stable SD and unstable SP grains. This relationship is made clear by data from TC (Fig. 7), which establish an explicit linkage between demagnetization behaviour, hysteresis properties, and the FORC distribution. As shown in Fig. 7a, stably magnetized samples that acquire GRMs at high AFs (TC08B; see also Fig. 3c) have low B_{cr}/B_c (<2) and $M_r/M_s \approx 0.5$, approaching SD-like values, whilst their FORC distributions also indicate a large population of magnetostatically interacting stable SD grains (GRM acquisition by SD greigite during AF demagnetization is a well-established phenomenon [e.g., 51]). Samples that still have a stable ChRM, but which do not acquire a GRM (TC28A; see also Fig. 3b) have elevated B_{cr}/B_c (≈ 3.5) and a FORC distribution similar to that seen for sample WU21A, with a large reversible ridge, thermal relaxation of the SD assemblage, and reduced magnetostatic interactions. Finally, samples from an unstably magnetized horizon (Fig. 3a), with no clear ChRM and $B_{cr}/B_c \geq 7$ (TC23A), have a FORC distribution almost exclusively consisting of thermally relaxed SP particles. Increasing B_{cr}/B_c also corresponds with wasp-waisted hysteresis loops (Fig. 7b), a further indication of an increasingly dominant SP contribution [48]. Normalized FORC profiles for representative samples from each of these groups (Fig. 7c) clearly show that as the relative height of the stable SD peak decreases, thermal relaxation effects become more dominant, shifting the higher coercivity distribution from a clear peak centred at ~60 mT to a flatter profile with lower B_c values. All of these observations are consistent with the increase in SP content indicated by comparison to theoretical SD-SP mixing curves (Fig. 7a), as is the increased relative magnitude of the reversible ridge (RR) in the profiles of Fig. 7c. A variable paramagnetic contribution due to lithological changes in the TC section (Fig. 3a) cannot be ruled out as the cause of variations in the magnitude of RR. Nevertheless, the increasing ratio between the two peaks of the FORC distribution (*RR/SD*, see inset in Fig. 7a) seems to provide a qualitative measure of the increasing SP component.

Further support for a common magnetic mineralogy in these samples comes from SEM observations (Fig. 8): abundant iron sulphides are seen in all samples, commonly forming aggregates with at least two distinct growth phases. The first generation consists of framboidal pyrite (P), often with euhedral overgrowths resulting from progressive recrystallization in evolving pore waters during early diagenesis [52]. Later generations of space-filling pyrite (P2) and greigite (G) have then grown around these framboids. The greigite invariably has a finer grain size than P2, and appears to have formed by neoformation on the surfaces of the earlier framboids (Fig. 8b, c, e and i) and silicate grains (Fig. 8l) or isolated patches in the spaces between the earlier

Fig. 8. Representative FORC distributions and back-scattered electron microscope images illustrating microtextures of authigenic greigite (G) and pyrite (P, P2). (a–c) Sample TC08AB, which (a) is dominated by thermally stable SD greigite, with strong magnetostatic interactions. A low *RR/SD* value indicates a small SP contribution (low reversible component of magnetization). (b) Typical iron sulphide aggregate, with neoformed greigite (G) on the surface of recrystallized early pyrite framboids (P), and a later space-filling pyrite generation (P2). (c) Higher magnification view of another aggregate with similar textural relationships. (d–f) Sample OR28A, showing (d) thermal relaxation of SD greigite due to a large SP population, indicated by elevated *RR/SD*. (e) Iron sulphide growth within a calcareous microfossil. Amorphous silica cement has grown around early pyrite (P), restricting growth of later iron sulphides (G, P2). (f) An early greigite framboid (G) rimmed by pyrite (P) and surrounded by silica cement. (g–i) Sample UB152A, which (g) contains thermally stable SD greigite. (h) Neoformation of greigite (G) between the cleavages of a detrital sheet silicate. (i) Aggregate consisting almost entirely of recrystallized pyrite framboids (P), with limited greigite neoformation (G) on their surfaces. (j–l) Sample NC06A, with (j) slight thermal relaxation of the SD population. (k) Iron sulphide aggregate volumetrically dominated by later iron sulphide generations (G, P2). (l) Greigite (G) neoformed on the surfaces of detrital silicate grains and surrounded by space-filling pyrite (P2). (m–o) Sample BG30A, which (m) is dominated by a large reversible component of magnetization, with negligible stable SD greigite. (n) Oxidized iron sulphide aggregate. (o) Close-up of the aggregate in (n) where later iron sulphide generations have been replaced by amorphous iron oxide. Early pyrite framboids (P) have also been partially affected.

framboids (Fig. 8e and k). These growth relationships suggest that the greigite either formed earlier than, or penecontemporaneously with, P2.

At OR, which is one of the localities where early remanence acquisition is verified by a fold test [36], early framboidal pyrite P is partially or completely

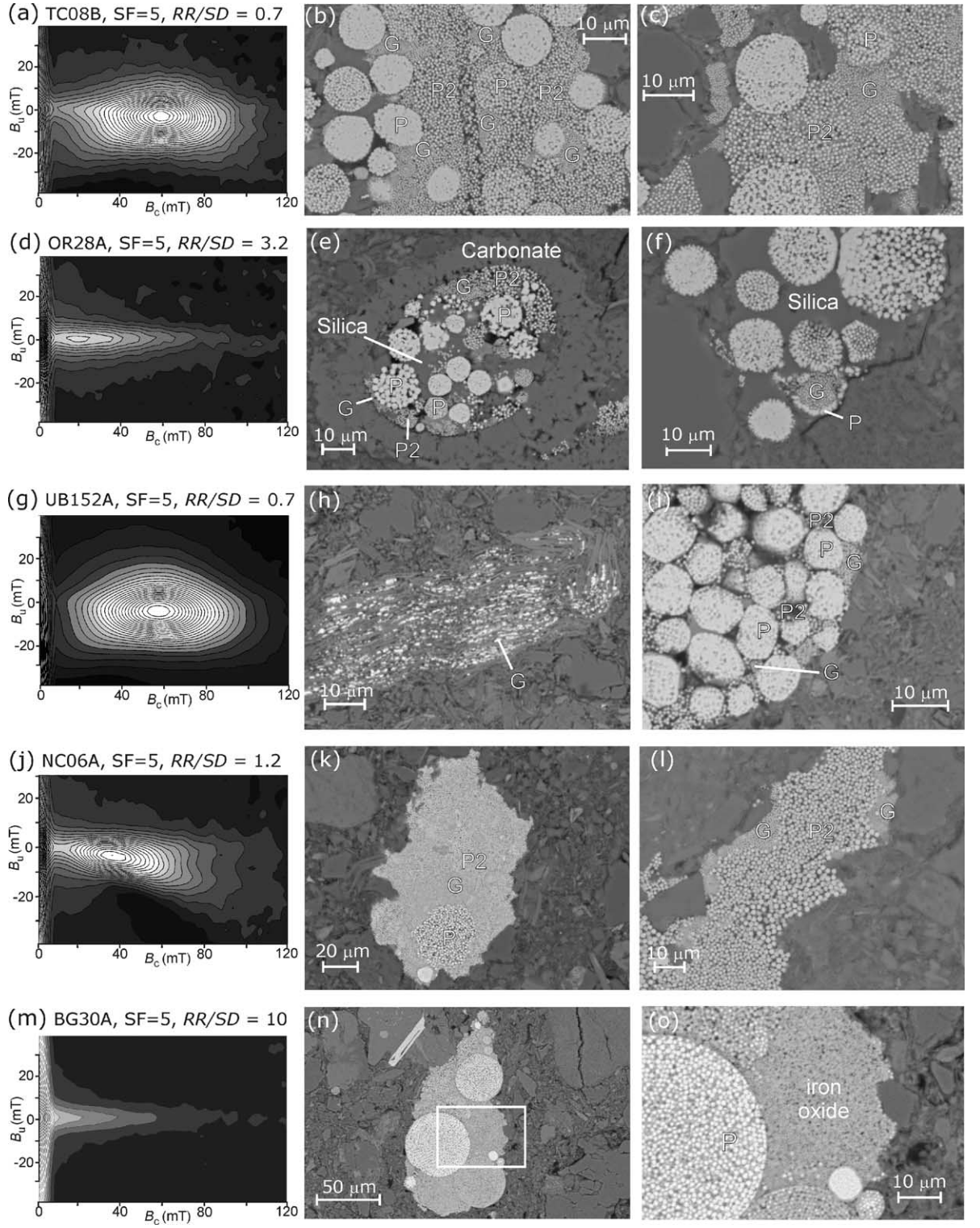

surrounded by amorphous silica cement (Fig. 8e and f), which appears to have limited the growth of later generations of iron sulphides. Where P2 and G have developed, the growth relationships appear to be similar to that described above; however, an earlier generation of greigite is also present as framboids rimmed by neoformed pyrite (Fig. 8f).

Neoformation of greigite between the cleavages of detrital sheet silicates (Fig. 8h) is also common in many samples. This has implications for the timing of remanence acquisition because, compared to magnetite, iron-bearing phyllosilicates are relatively unreactive to sulphide, requiring thousands of years for partial dissolution to occur [26,29,35].

In many samples, EDS analyses of the iron sulphides reveal elevated Fe/S ratios and measurable oxygen peaks in the absence of silicate and carbonate minerals, suggesting that they are oxidized to some degree. At sites where there is no trace of an ancient paleomagnetic signal, this oxidation has extensively degraded later iron sulphides, replacing them with amorphous iron oxide (Fig. 8n and o). The FORC distributions for such samples are dominated by a large reversible component of magnetization (Fig. 8m).

5. Discussion

Paleomagnetic data demonstrate that the magnetizations of Neogene sediments from New Zealand are often complex. The late-forming (>1 Myr after deposition) CRMs on Mahia Peninsula and Waihau Beach require involvement of an authigenic phase, such as greigite, but our SEM observations also link greigite with early-forming remanences in the Rakauroa and Marlborough regions. The samples share certain aspects of their demagnetization behaviour, particularly magnetic unblocking above 250 °C, the onset of thermal alteration at ~350 °C, and a general unresponsiveness to AF treatment, with many other New Zealand Cenozoic mudstones, which suggests that fine-grained greigite may be common in these rocks.

Our observations contrast with previous studies, which have generally failed to definitively identify the dominant magnetic carrier [14,19,27]. Because the remanence is generally carried by small amounts of greigite, obtaining sufficiently clean magnetic extracts to enable detection by XRD would be difficult. The FORC profile of sample UB192A (Fig. 6c), where greigite was detected by XRD [19], has an absolute magnetic moment that is an order of magnitude higher than that of most other samples, exemplified by sample WU21A (Fig. 6c and d); clear identification of greigite is therefore much simpler for samples like UB192A. However, such high concentrations of thermally stable greigite appear to be relatively rare in New Zealand sediments. Greigite is also typically a fine-grained component in the space-filling matrix of iron sulphide aggregates (Fig. 8), which might not survive the extraction process intact, leaving the more robust and/or volumetrically more significant pyrite framboids. This may explain the presence of pyrite in magnetic extracts, just as observations of greigite within chlorite cleavages (Fig. 8h) might explain the common occurrence of chlorite in extracts in which greigite has been identified [19].

The magnetic properties of these sediments are dominantly controlled by variable mixtures of SP and stable SD material, with a large SP component being common. The lack of any other identified magnetic minerals strongly suggests that greigite is also responsible for the SP signal. Greigite formation involves in situ nucleation and growth of ferrimagnetic grains; any individual grain must therefore initially be small and magnetically SP, before growing through the stable SD blocking volume and becoming capable of preserving a thermally stable ChRM. During the early stages of growth, most particles will be SP, with only a small number of larger grains having SD magnetic properties (Fig. 9a). With unlimited growth, all particles will eventually become SD; however, even when the average grain size moves past the SD threshold volume, significant amounts of SP material can remain in the rock (Fig. 9b). The magnetic signature of these samples is therefore consistent with populations of authigenic greigite, with variable grain size distributions ranging across the critical boundary for SP/SD behaviour. Differing proportions of SP and SD grains (Fig. 6e) appear to have resulted from greigite growth being arrested at slightly different times. A plot of the ratio *RR/SD* against B_{cr}/B_c for all studied samples (Fig. 9d) indicates that in the majority of cases, growth appears to have been arrested at a relatively early stage, resulting in the preservation of large amounts of SP greigite, FORC distributions centred near the origin, and elevated B_{cr}/B_c ratios. The relatively small amounts of stable SD greigite lead to weak NRMs. In some horizons at TC, and at many of the Marlborough localities, growth of greigite has progressed further, such that SD particles begin to dominate (Figs. 6a, 8a and g, and 9c). At the other extreme, samples from unstably magnetized horizons at TC and NR have high *RR/SD* ratios and large reversible components on their FORC distributions (e.g., NR08A, Fig. 9d), which is consistent with the presence of a large population of SP grains and may therefore represent greigite populations 'frozen' in the

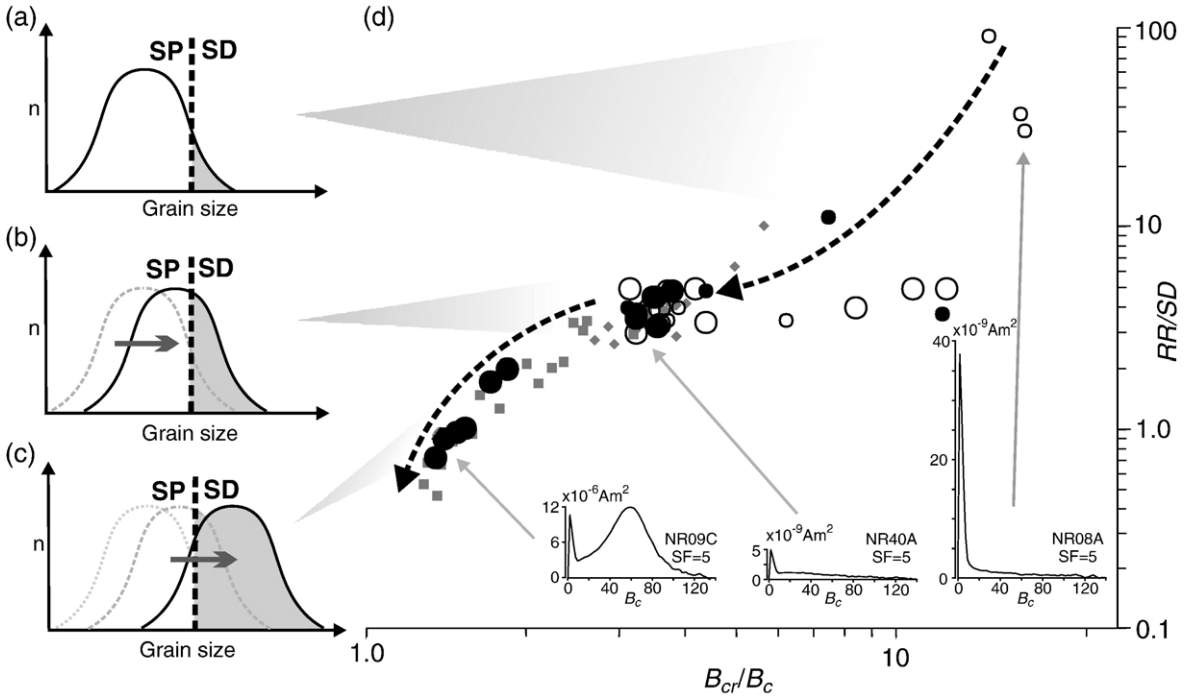

Fig. 9. (a–c) Illustration of the progressive authigenic growth of greigite. (a) Just after initiation of growth, all grains are small, and most will therefore be SP. (b) As the average grain size increases with further growth, a larger amount of greigite attains the blocking volume for stable SD behaviour and can potentially retain a ChRM. A large SP population remains, however. (c) After the average grain size has moved past the blocking volume, SD grains begin to dominate the mixture. These distributions are linked to the relevant region of (d), a plot of $\boldsymbol{B}_{cr}/\boldsymbol{B}_c$ against *RR/SD*, which is a qualitative measure of the relative proportions of SP and SD material in a sample. FORC profiles of samples at each stage of growth are inset for further clarification. Data from Mahia Peninsula (closed circles = normal polarity samples, open circles = reversed polarity, small circles = unstably magnetized) and Marlborough (squares) have been separated from data for other localities from the east coast of the North Island (diamonds). Greigite in most samples is still dominantly SP, apparently due to the early arrest of authigenic growth.

early stages of growth (Fig. 9a). The ability of rock magnetic measurements to constrain the varying proportions of SD and SP greigite in these rocks is of great potential importance; more detailed SEM analysis of grain size distributions may allow the threshold size for stable SD behaviour of greigite, which is currently poorly constrained, to be determined.

The factors governing the arrest of pyritization and consequent preservation of greigite in these sediments are still not fully understood. There are clearly some lithological controls on this process, however. On the Mahia Peninsula, the older, reversed polarity, CRM is generally found in beds rich in volcanic material, whereas the later, normal polarity magnetization is associated with mudstone units (e.g., Fig. 3i). Furthermore, localities with abundant stable SD greigite tend to consist of very fine-grained mudstones rather than the coarser siltstones and mudstones that dominate elsewhere in the Neogene sedimentary basins of New Zealand. These observations suggest that authigenic growth is being limited by underlying chemical controls. Geochemical analyses of fine-grained sediments from Taiwan that are magnetically dominated by stable SD greigite suggest that greigite preservation is favoured by a combination of limited organic carbon, which limits microbial production of dissolved sulphide, and high concentrations of reactive iron [30]. In later diagenetic sulphidization events, sulphate limitation, by closure of the system to seawater due to burial, may also be a factor. Geochemical analyses of New Zealand sediments are required to identify the mechanisms controlling greigite growth and grain size.

SEM analyses have also cast light on the source of the strong viscous overprints that are common in New Zealand Cenozoic sediments. In previous studies, unanchored demagnetization paths have indicated the presence of a high-temperature magnetic component that is thought to be carried by iron oxides such as hematite [14]. Our observations of iron oxides replacing authigenic iron sulphides (Fig. 8n and o) demonstrate that these oxides, although not necessarily hematite, also have an authigenic origin, and that they are most likely a product of pyrite oxidation in percolating oxic ground water. Greigite, as the finest

grained iron sulphide phase, will also be highly reactive; the oxidation process will therefore involve replacement of SP and SD greigite, as well as paramagnetic pyrite, by SP iron oxides. As discussed above, authigenic growth produces large populations of SP grains, and magnetic viscosity associated with high concentrations of SP hematite is a well-documented phenomenon [53]. Samples from the Rakauroa localities, and from WH and BG (Fig. 1c), where a strong viscous overprint is observed, have reduced M_r/M_s, consistent with the presence of additional SP hematite (Fig. 6e). Furthermore, at localities AB, WH and BG, where there is no identifiable ChRM beneath the overprint, samples have FORC distributions with a negligible SD component (Fig. 8m) and progressively increased B_{cr}/B_c indicative of increasing SP grain size (Fig. 6e); these changes are consistent with continued growth of SP iron oxides at the expense of SD greigite. Unfortunately, however, these variations are within the range observed at localities lacking a significant viscous component (Fig. 6e); strongly overprinted samples therefore cannot be identified by rock magnetic measurements alone.

Perhaps the most significant results of our study relate to the timing of greigite formation. In two instances, we have clearly shown that remanence acquisition post-dates deposition by >1 Myr; caution is therefore required when using paleomagnetic data for tectonic studies of the Hikurangi Margin. For example, when properly corrected, synfolding magnetizations from the Mahia Peninsula indicate $44 \pm 5^\circ$ of tectonic rotation since 4–6 Ma, which requires a much higher rate of rotation than has been previously inferred [6,9]. Late-forming greigite may be common, and if it is not identified, both the rate and magnitude of tectonic rotations will be underestimated; this was the case at WU, where an earlier study found only the late-forming magnetization and incorrectly assumed that it was primary [31,54].

However, even at localities where greigite appears to have formed relatively early, multiple generations of iron sulphide growth, with later generations often being volumetrically dominant (e.g., Fig. 8b and k), as well as sulphidization of phyllosilicates (e.g., Fig. 8h) both appear to require sulphide growth over a significant period of time following deposition, potentially tens of thousands of years in the latter case [26]. Such a delay is well within the constraints provided by field tests, which often still allow a considerable period of time for remanence acquisition. The magnetizations at Rakauroa are only constrained to within 1–2 Myr of deposition by a fold test [36], although greigite associated with the first generation of framboids at OR (Fig. 8f) does suggest early growth. Protection of this early greigite generation by the surrounding amorphous silica cement might have contributed to the preservation of a pre-folding remanence. In Marlborough, paleomagnetically determined crustal rotations are systematically lower than the rotations seen in the underlying Torlesse basement fabric [11], although both estimates are generally within error of each other. This discrepancy might also be due to delayed remanence acquisition in the Neogene sediments, but other explanations are also possible (e.g., rotations occurring prior to deposition of the sedimentary cover). Nonetheless, our observations suggest that in New Zealand Cenozoic marine sediments a truly syn-depositional paleomagnetic signal is rarely preserved intact. At best, greigite that formed during later phases of sulphide growth is restricted and is volumetrically dominated by earlier greigite, as has been documented for greigite-bearing sediments in Italy [55].

Delays in remanence acquisition of even a few thousand years have potentially serious consequences for studies of short-period geomagnetic field behaviour. Even more troubling are the implications for magnetostratigraphy of results from the WU and NR localities, where two differently timed magnetizations are patchily distributed at outcrop scale, producing a spurious apparent reversal sequence. The fact that similar patchy remagnetizations, involving late greigite growth and giving rise to false 'reversal' sequences, have been observed elsewhere [33] suggests that this is not an isolated phenomenon. Furthermore, discriminating between earlier and later forming magnetizations appears to be difficult in the absence of paleomagnetic constraints: at WU, neither SEM observations [31] nor rock magnetic measurements (Fig. 6) provide any clear means of discriminating between horizons with early and late formed greigite. Stably magnetized samples of both polarities at NR also cannot be distinguished by their magnetic properties (Fig. 9d). Unlike at WU, the fact that the two polarities formed at different times only became evident following the addition of paleomagnetic data from nearby localities; if samples from this locality were analyzed in isolation, the difference in mean directions is small enough that they might easily be thought to record a primary sequence of reversals.

It is possible that other techniques, particularly geochemical analysis (e.g., laser ablation $\delta^{34}S$ analysis on polished sections), might allow early- and late-forming greigite to be distinguished in these sediments. Currently, however, in the absence of diagnostic indicators

from rock magnetic and SEM analyses, the use of paleomagnetic field tests to constrain the age of remanence acquisition of greigite is essential. Furthermore, the reversals test should be used with extreme care: the existence of apparent reversal stratigraphies resulting from patchy, differently timed remagnetizations involving greigite indicate that a positive reversals test is not necessarily diagnostic of an early magnetization.

Late remagnetizations involving greigite are not confined to New Zealand. Inconsistent geomagnetic polarities associated with later-forming greigite have been reported from Plio-Pleistocene sequences in Taiwan [35,56] and the New Jersey margin [57], Miocene glaciomarine sediments from Antarctica [33], and fine-grained Neogene sediments on the Italian peninsula [34], where ferrimagnetic iron sulphides are widespread [58], and where paleomagnetic data from greigite-bearing sediments have also been used to infer tectonic rotations [59]. It is becoming apparent that conditions amenable to greigite preservation are common in rapidly deposited continental margin deposits, which are often targeted for high-resolution studies of geomagnetic field behaviour. If greigite is present in these sequences, the possibility that the paleomagnetic record has been compromised by delayed remanence acquisition must be seriously considered.

6. Conclusions

Paleomagnetic measurements, combined with detailed rock magnetic and SEM analyses, demonstrate that the authigenic iron sulphide, greigite, which forms during reductive diagenesis, is a common remanence carrier in New Zealand Cenozoic mudstones. Although greigite can form during early diagenesis, in at least two instances authigenic growth has occurred >1 Myr after deposition. The resulting late remagnetizations can be irregularly distributed within an outcrop, and cannot be readily distinguished from earlier magnetizations by either SEM observations or by rock magnetic measurements. Remanent magnetizations are further affected by pyrite and greigite oxidation in oxic ground waters, forming fine-grained iron oxides that carry a dominant viscous overprint. Progressive oxidation of the iron sulphides eventually destroys any older paleomagnetic signal.

Late remagnetizations may seriously impact upon the reliability of magnetostratigraphic and tectonic studies, not only in the New Zealand region but also in similar sequences worldwide. In the light of our observations, a priori assumption of early remanence acquisition in sediments where greigite is present is extremely risky in the absence of confirmation from paleomagnetic field tests. Even an apparent reversal sequence can result from patchily distributed, diachronous magnetizations; the most reliable constraints come from structural field tests.

Acknowledgements

This research was supported by contributions from the UK Natural Environment Research Council (grant NER/S/2001/06363), the Leverhulme Trust, and the Royal Society of London. We thank R. Pearce, Y. Iizuka and Y.H. Shau for invaluable assistance with SEM analysis, L. Carter for providing access to core MD972121, Joe Colliver and Kevin Padley for laboratory assistance, and L. Sagnotti, M. Dekkers and an anonymous reviewer for helpful comments that improved this paper.

References

[1] J.P. Kennett, N.D. Watkins, Late Miocene–Early Pliocene paleomagnetic stratigraphy, paleoclimatology, and biostratigraphy in New Zealand, Geol. Soc. Amer. Bull. 85 (1974) 1385–1398.
[2] B.R. Lienert, D.A. Christoffel, P. Vella, Geomagnetic dates on a New Zealand Upper Miocene–Pliocene section, Earth Planet. Sci. Lett. 16 (1972) 195–199.
[3] A.P. Roberts, G.M. Turner, P.P. Vella, Magnetostratigraphic chronology of Late Miocene to Early Pliocene biostratigraphic and oceanographic events in New Zealand, Geol. Soc. Amer. Bull. 106 (1994) 665–683.
[4] R.I. Walcott, D.A. Christoffel, T.C. Mumme, Bending within the axial tectonic belt of New Zealand in the last 9 Myr from paleomagnetic data, Earth Planet. Sci. Lett. 52 (1981) 427–434.
[5] T.C. Mumme, R.I. Walcott, Paleomagnetic Studies at Geophysics Division 1980–1983, Department of Scientific and Industrial Research, Wellington, New Zealand, 1985.
[6] I.C. Wright, R.I. Walcott, Large tectonic rotation of part of New Zealand in the past 5 Ma, Earth Planet. Sci. Lett. 80 (1986) 348–352.
[7] S.H. Lamb, H.M. Bibby, The last 25 Ma of rotational deformation in part of the New Zealand plate boundary zone, J. Struct. Geol. 11 (1989) 473–492.
[8] T.C. Mumme, S. Lamb, R.I. Walcott, The Raukumara paleomagnetic domain: constraints on the tectonic rotation of the East Coast, N Island, New Zealand, from paleomagnetic data, N.Z. J. Geol. Geophys. 32 (1989) 317–326.
[9] R.I. Walcott, Paleomagnetically observed rotations along the Hikurangi Margin of New Zealand, in: C. Kissel, C. Laj (Eds.), Paleomagnetic Rotations and Continental Deformation, Kluwer, Dordrecht, 1989, pp. 459–471.
[10] A.P. Roberts, Paleomagnetic constraints on the tectonic rotation of the southern Hikurangi margin, New Zealand, N.Z. J. Geol. Geophys. 35 (1992) 311–323.
[11] T.A. Little, A.P. Roberts, Distribution and mechanism of Neogene to present-day vertical axis rotations, Pacific–Australian

plate boundary zone, South Island, New Zealand, J. Geophys. Res. 102 (1997) 20447–20468.
[12] L.M. Wallace, J. Beavan, R. McCaffrey, D. Darby, Subduction zone coupling and tectonic block rotations in the North Island, New Zealand, J. Geophys. Res. 109 (2004) 406–427.
[13] J. Beavan, J. Haines, Contemporary horizontal velocity and strain rate fields of the Pacific–Australian plate boundary zone through New Zealand, J. Geophys. Res. 106 (2001) 741–770.
[14] G.M. Turner, Toward an understanding of the multicomponent magnetization of uplifted marine sediments in New Zealand, J. Geophys. Res. 106 (2001) 6385–6397.
[15] P.R. King, Tectonic reconstructions of New Zealand: 40 Ma to the present, N.Z. J. Geol. Geophys. 43 (2000) 611–638.
[16] G.J. Rait, F. Chanier, D.W. Waters, Landward- and seaward-directed thrusting accompanying the onset of subduction beneath New Zealand, Geology 19 (1991) 230–233.
[17] T.C. Mackinnon, Origin of the Torlesse Terrane and coeval rocks, South Island, New Zealand, Geol. Soc. Amer. Bull. 94 (1983) 967–985.
[18] D. Smale, Distribution and provenance of heavy minerals in the South Island—a review, N.Z. J. Geol. Geophys. 33 (1990) 557–571.
[19] A.P. Roberts, G.M. Turner, Diagenetic formation of ferrimagnetic iron sulphide minerals in rapidly deposited marine sediments, South Island, New Zealand, Earth Planet. Sci. Lett. 115 (1993) 257–273.
[20] L. Carter, P. Shane, B. Alloway, I.R. Hall, S.E. Harris, J.A. Westgate, Demise of one volcanic zone and birth of another—a 12 m.y. marine record of major rhyolitic eruptions from New Zealand, Geology 31 (2003) 493–496.
[21] L. Carter, B. Manighetti, M. Elliot, N. Trustrum, B. Gomez, Source, sea level and circulation effects on the sediment flux to the deep ocean over the past 15 ka off eastern New Zealand, Global Planet, Change 33 (2002) 339–355.
[22] R.A. Berner, Sedimentary pyrite formation—an update, Geochim. Cosmochim. Acta 48 (1984) 605–615.
[23] R. Karlin, S. Levi, Geochemical and sedimentological control of the magnetic properties of hemipelagic sediments, J. Geophys. Res. 90 (1985) 373–392.
[24] R. Karlin, S. Levi, Diagenesis of magnetic minerals in recent haemipelagic sediments, Nature 303 (1983) 327–330.
[25] R. Karlin, Magnetite diagenesis in marine sediments from the Oregon continental margin, J. Geophys. Res. 95 (1990) 4405–4419.
[26] D.E. Canfield, R. Raiswell, S. Bottrell, The reactivity of sedimentary iron minerals toward sulfide, Am. J. Sci. 292 (1992) 659–683.
[27] G.S. Wilson, A.P. Roberts, Diagenesis of magnetic mineral assemblages in multiply redeposited siliciclastic marine sediments, Wanganui Basin, New Zealand, in: D.H. Tarling, P. Turner (Eds.), Paleomagnetism and Diagenesis in Sediments, Geol. Soc. Spec. Publ., vol. 151, 1999, pp. 95–108.
[28] R.T. Wilkin, H.L. Barnes, Formation processes of framboidal pyrite, Geochim. Cosmochim. Acta 61 (1997) 323–339.
[29] A.P. Roberts, R. Weaver, Multiple mechanisms of remagnetization involving sedimentary greigite (Fe_3S_4), Earth Planet. Sci. Lett. 231 (2005) 263–277.
[30] S.J. Kao, C.S. Horng, A.P. Roberts, K.K. Liu, Carbon–sulfur–iron relationships in sedimentary rocks from southwestern Taiwan: influence of geochemical environment on greigite and pyrrhotite formation, Chem. Geol. 203 (2004) 153–168.
[31] C.J. Rowan, A.P. Roberts, Tectonic and geochronological implications of variably timed magnetizations carried by authigenic greigite in marine sediments from New Zealand, Geology 33 (2005) 553–566.
[32] A.P. Roberts, B.J. Pillans, Rock magnetism of Lower–Middle Pleistocene marine sediments, Wanganui Basin, New Zealand, Geophys. Res. Lett. 20 (1993) 839–842.
[33] L. Sagnotti, A.P. Roberts, R. Weaver, K.L. Verosub, F. Florindo, C.R. Pike, T. Clayton, G.S. Wilson, Apparent magnetic polarity reversals due to remagnetization resulting from late diagenetic growth of greigite from siderite, Geophys. J. Int. 160 (2005) 89–100.
[34] F. Florindo, L. Sagnotti, Palaeomagnetism and rock magnetism in the Upper Pliocene Valle Ricca (Rome, Italy) section, Geophys. J. Int. 123 (1995) 340–354.
[35] W.T. Jiang, C.S. Horng, A.P. Roberts, D.R. Peacor, Contradictory magnetic polarities in sediments and variable timing of neoformation of authigenic greigite, Earth Planet. Sci. Lett. 193 (2001) 1–12.
[36] C.J. Rowan, A.P. Roberts, G.J. Rait, Relocation of the tectonic boundary between the Raukumara and Wairoa domains (East Coast, North Island, New Zealand): implications for the rotation history of the Hikurangi margin, N.Z. J. Geol. Geophys. 48 (2005) 185–196.
[37] C.R. Pike, A.P. Roberts, K.L. Verosub, Characterizing interactions in fine magnetic particle systems using first order reversal curves, J. Appl. Phys. 85 (1999) 6660–6667.
[38] A.P. Roberts, C.R. Pike, K.L. Verosub, First-order reversal curve diagrams: a new tool for characterizing the magnetic properties of natural samples, J. Geophys. Res. 105 (2000) 28461–28475.
[39] C. Mazengarb, I.G. Speden, Geology of the Raukumara Area. 1: 250 000 geological map 6, Institute of Geological and Nuclear Sciences Limited, Lower Hutt, New Zealand, 2000.
[40] C. Buret, F. Chanier, J. Ferriere, J.N. Proust, Individualization of a forearc basin during the active margin evolution: Hikurangi subduction margin, New Zealand, C. R. Acad. Sci., Ser. IIA 325 (1997) 615–621.
[41] P.L. McFadden, M.W. McElhinny, Classification of the reversal test in palaeomagnetism, Geophys. J. Int. 103 (1990) 725–729.
[42] L. Tauxe, G. Watson, The fold test: an eigen analysis approach, Earth Planet. Sci. Lett. 122 (1994) 331–341.
[43] M. Idnurm, Late Mesozoic and Cenozoic palaeomagnetism of Australia. 1. A redetermined apparent polar wander path, Geophys. J. R. Astron. Soc. 83 (1985) 399–418.
[44] G.M. Turner, A.P. Roberts, C. Laj, C. Kissel, A. Mazaud, S. Guitton, D.A. Christoffel, New paleomagnetic results from Blind River—revised magnetostratigraphy and tectonic rotation of the Marlborough region, South Island, New Zealand, N.Z. J. Geol. Geophys. 32 (1989) 191–196.
[45] A.P. Roberts, Magnetic properties of sedimentary greigite (Fe_3S_4), Earth Planet. Sci. Lett. 134 (1995) 227–236.
[46] C.R. Pike, First-order reversal curve diagrams and reversible magnetization, Phys. Rev., B 68 (2003) (art. no. 104424).
[47] C.R. Pike, A.P. Roberts, K.L. Verosub, First-order reversal curve diagrams and thermal relaxation effects in magnetic particles, Geophys. J. Int. 145 (2001) 721–730.
[48] L. Tauxe, T.A.T. Mullender, T. Pick, Potbellies, wasp-waists, and superparamagnetism in magnetic hysteresis, J. Geophys. Res. 101 (1996) 571–583.
[49] D.J. Dunlop, Theory and application of the Day plot (M_{rs}/M_s versus H_{cr}/H_c) 1. Theoretical curves and tests using titano-

magnetite data, J. Geophys. Res. 107 (2002), (2056) doi:10.1029/2001JB000486.

[50] R. Day, M. Fuller, V.A. Schmidt, Hysteresis properties of titanomagnetites: grain size and composition dependence, Phys. Earth Planet. Inter. 13 (1977) 260–266.

[51] I.F. Snowball, Gyroremanent magnetization and the magnetic properties of greigite-bearing clays in southern Sweden, Geophys. J. Int. 129 (1997) 624–636.

[52] R. Raiswell, Pyrite texture, isotopic composition and the availability of iron, Am. J. Sci. 282 (1982) 1244–1263.

[53] K.M. Creer, Superparamagnetism in red sandstones, Geophys. J. R. Astron. Soc. 5 (1961) 16–28.

[54] S. Thornley, Neogene Tectonics of Raukumara Peninsula, Northern Hikurangi Margin, New Zealand, Unpublished PhD thesis, Victoria University of Wellington, 1996.

[55] A.P. Roberts, W.T. Jiang, F. Florindo, C.S. Horng, C. Laj, Assessing the timing of greigite formation and the reliability of the Upper Olduvai polarity transition record from the Crostolo River, Italy, Geophys. Res. Lett. 32 (2005), (L05307) doi:10.1029/2004GL022137.

[56] C.S. Horng, M. Torii, K.S. Shea, S.J. Kao, Inconsistent magnetic polarities between greigite and pyrrhotite/magnetite-bearing marine sediments from the Tsailiao-chi section, southwestern Taiwan, Earth Planet. Sci. Lett. 164 (1998) 467–481.

[57] H. Oda, M. Torii, Sea-level change and remagnetization of continental shelf sediments off New Jersey (ODP Leg 174A): magnetite and greigite diagenesis, Geophys. J. Int. 156 (2004) 443–458.

[58] L. Sagnotti, A. Winkler, Rock magnetism and palaeomagnetism of greigite-bearing mudstones in the Italian peninsula, Earth Planet. Sci. Lett. 165 (1999) 67–80.

[59] F. Speranza, L. Sagnotti, M. Mattei, Tectonics of the Umbria–Marche–Romagna Arc (central northern Apennines, Italy): new paleomagnetic constraints, J. Geophys. Res. 102 (1997) 3153–3166.